Kinetic models for wave propagation in random media

II. Validity and Applications

Guillaume Bal

Department of Applied Physics & Applied Mathematics

Columbia University

http://www.columbia.edu/~gb2030

gb2030@columbia.edu

Outline for Lecture I.

1. Waves in heterogeneous media
2. High Frequency regime and Geometrical optics
3. Wigner transforms
4. Radiative Transfer model in the weak coupling regime
5. Random Liouville, paraxial and Itô-Schrödinger approximations
6. More general Radiative Transfer models

Outline for Lecture II.

1. **Time Reversal in random media**

2. Statistical stability

3. Validity of Radiative Transfer Models

4. Applications to Detection and Imaging

Time Reversal framework

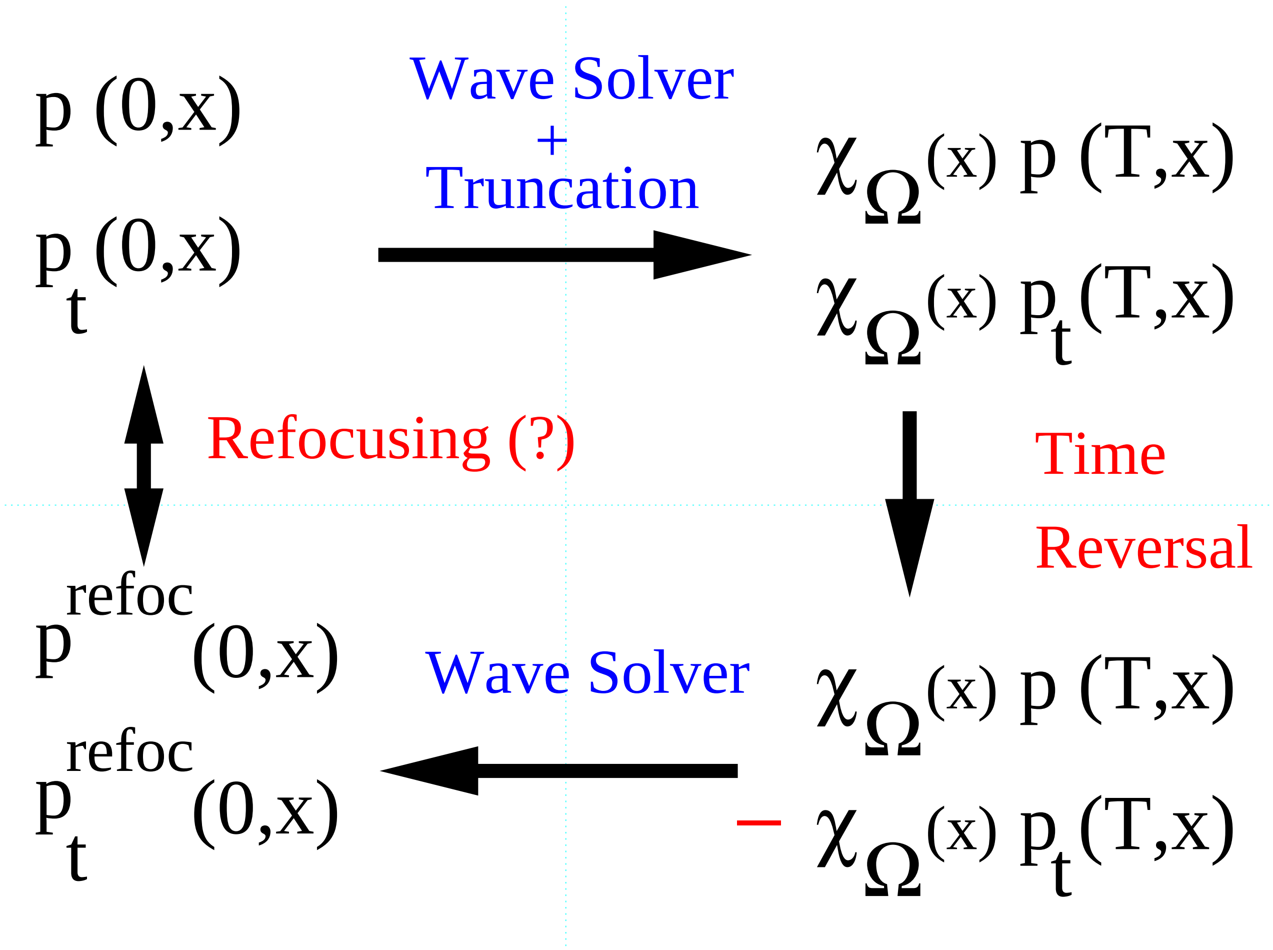

Numerical Experiment: Initial Data

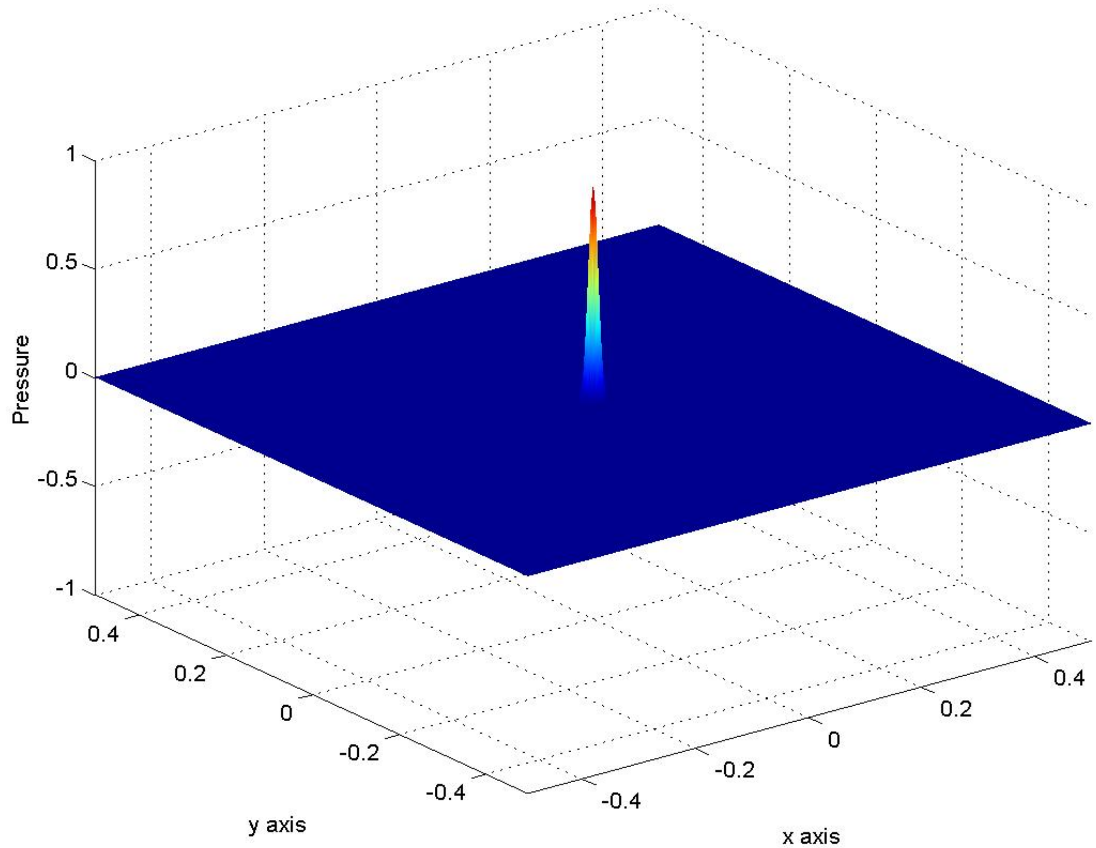

Numerical Experiment: Forward Solution

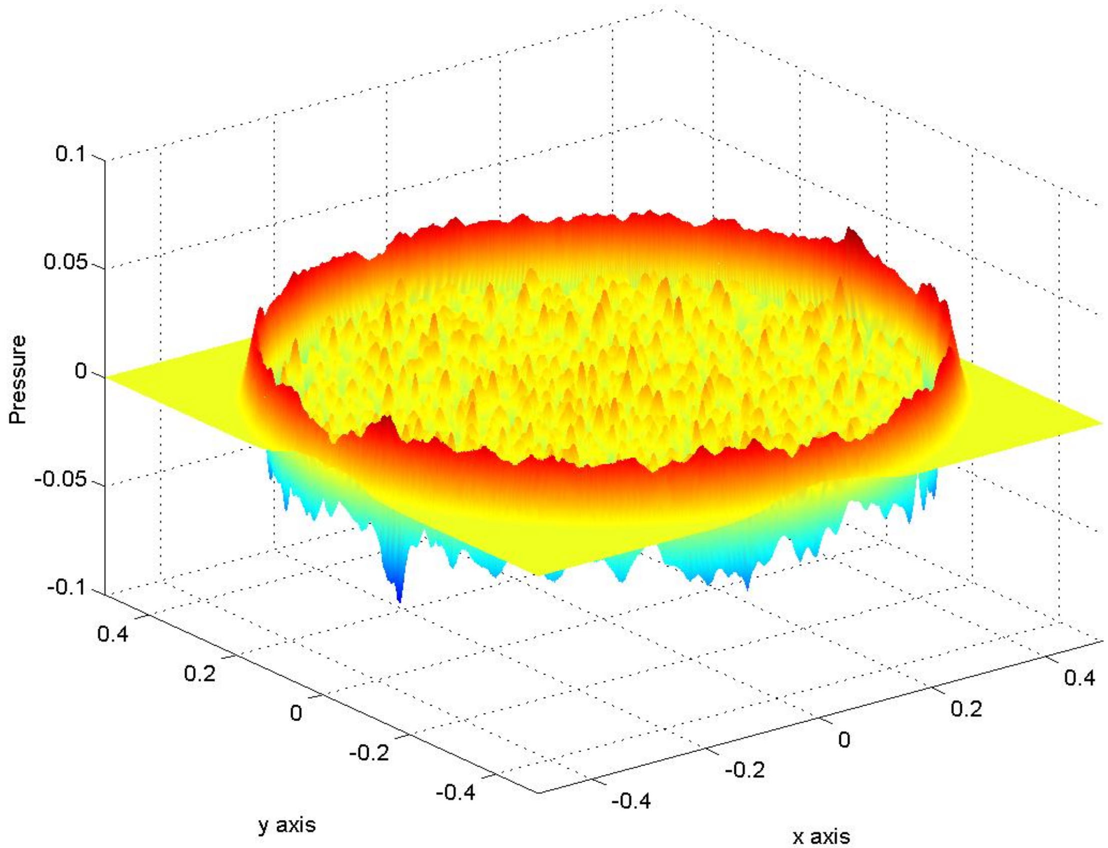

Numerical Experiment: Truncated Solution

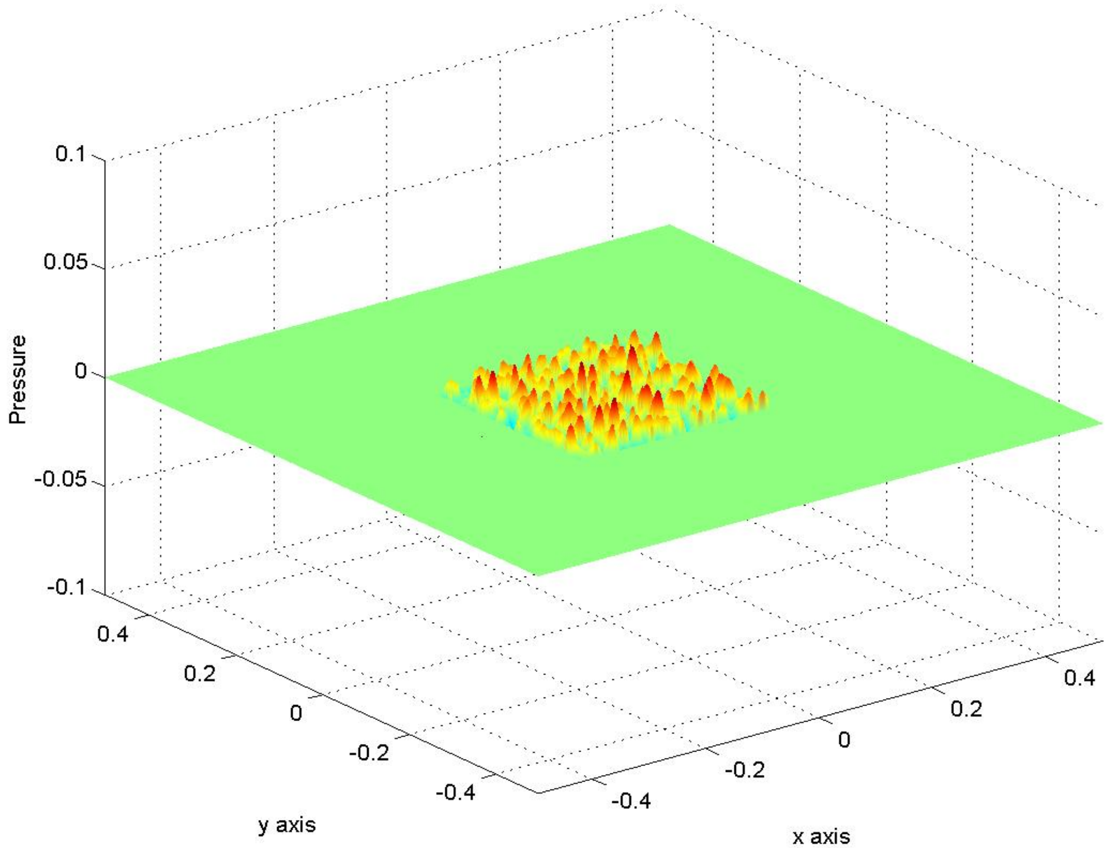

Numerics: Time-reversed Solution

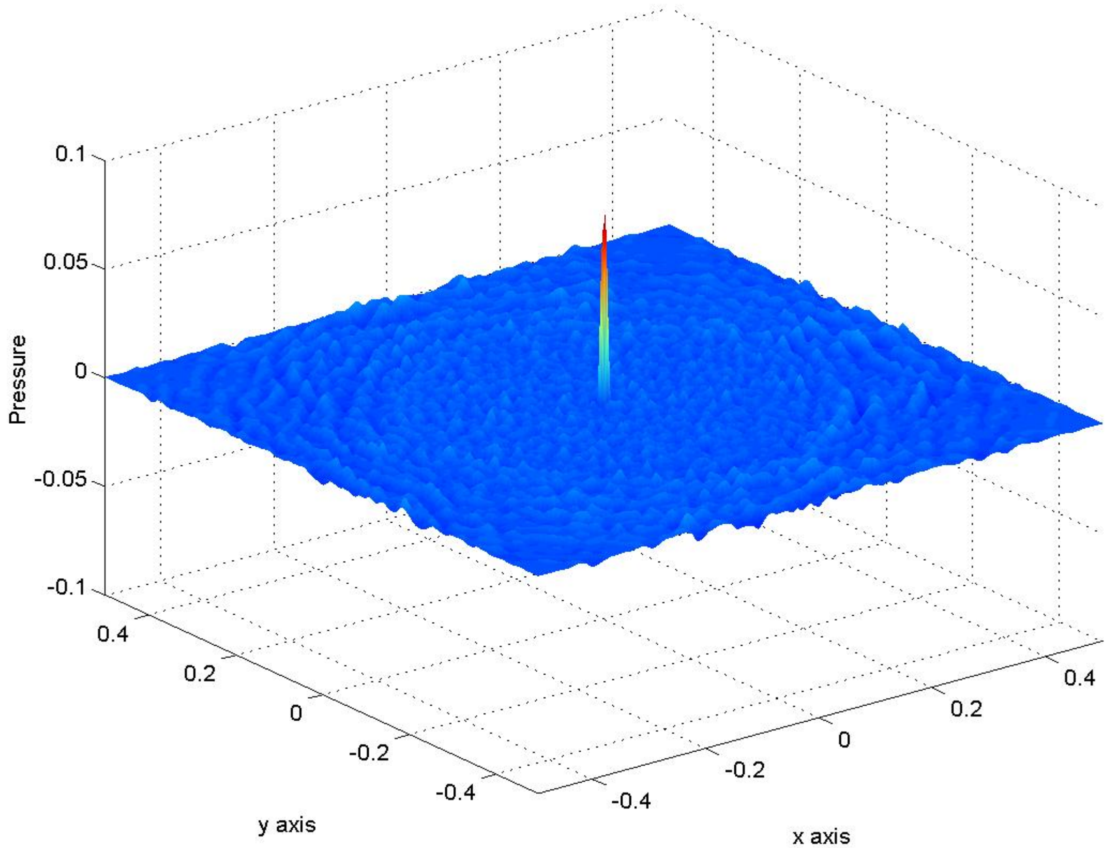

Zoom on Refocused and Original Signals

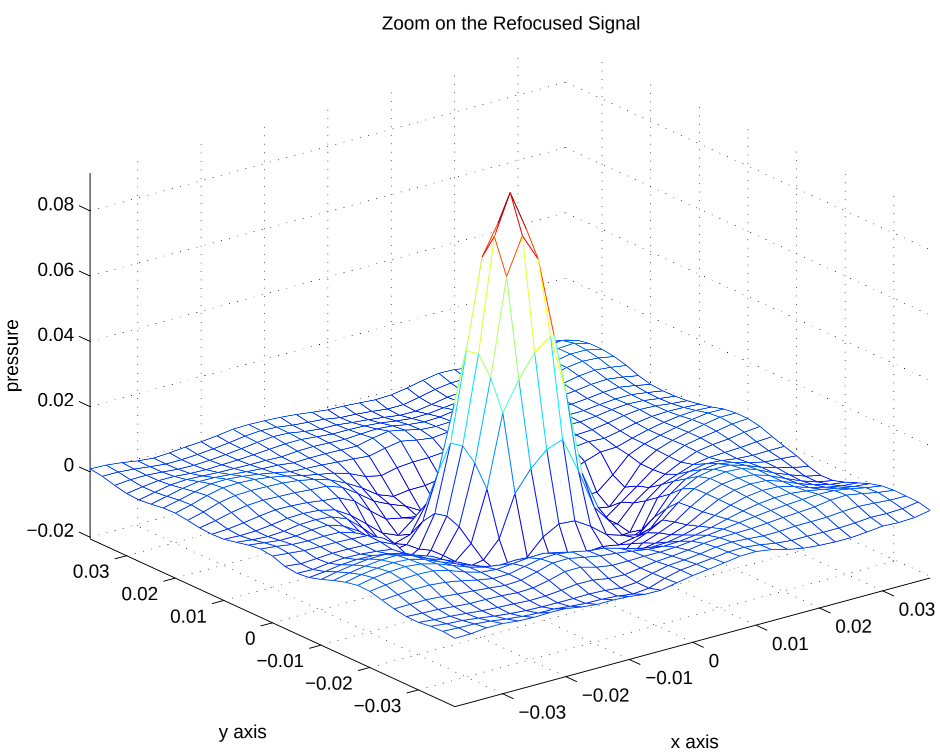

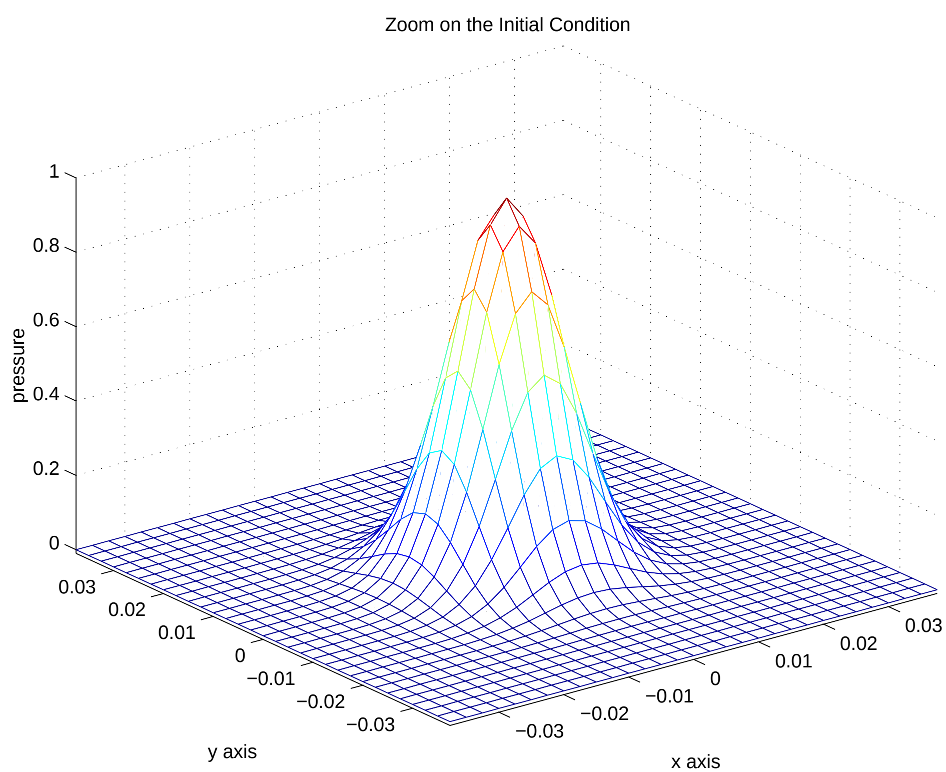

Time-reversal in changing 3D media

We consider time reversal with possibly a change of medium between the forward ($\varphi = 1$) and backward ($\varphi = 2$) stages. The forward problem for $\mathbf{u}^\varphi = (\mathbf{v}, p) = (v_1, v_2, v_3, p)$ is

$$A^\varphi(\mathbf{x})\frac{\partial \mathbf{u}^\varphi(t,\mathbf{x})}{\partial t} + D^j \frac{\partial \mathbf{u}^\varphi(t,\mathbf{x})}{\partial x_j} = 0, \quad \mathbf{x} \in \mathbb{R}^3, \quad \varphi = 1, 2,$$

with initial condition $\mathbf{u}^1(t=0) = \mathbf{u}_0$; $\underline{A^\varphi(\mathbf{x}) = \mathrm{Diag}(\rho, \rho, \rho, \kappa^\varphi(\mathbf{x}))}$.

Using Green's propagators $G^\varphi(t, \mathbf{x}; \mathbf{y})$, the back-propagated signal is

$$\boxed{\mathbf{u}^B(\mathbf{x}) = \int_{\mathbb{R}^9} \Gamma G^2(T, \mathbf{x}; \mathbf{y}) \Gamma G^1(T, \mathbf{y}'; \mathbf{z}) \chi_\Omega(\mathbf{y}) \chi_\Omega(\mathbf{y}') f(\mathbf{y} - \mathbf{y}') \mathbf{u}_0(\mathbf{z}) d\mathbf{y} d\mathbf{y}' d\mathbf{z}.}$$

- $\Gamma = \mathrm{Diag}(-1, -1, -1, 1)$ models the time reversal process
- $\chi_\Omega(\mathbf{y})$ models the array of detectors and $f(\mathbf{y})$ blurring at the detectors
- T is the duration of each propagation stages.

High Frequency scaling

We are interested in high frequency ($O(\varepsilon^{-1})$) wave propagation and thus wish to analyze the refocusing signal at distances $O(\varepsilon)$ away from the source center.

Rescale the problem with $\mathbf{u}_0(\mathbf{x}) = \mathbf{S}\left(\frac{\mathbf{x}-\mathbf{x}_0}{\varepsilon}\right)$ and accordingly with a filter $\frac{1}{\varepsilon^d} f(\frac{\mathbf{y}-\mathbf{y}'}{\varepsilon})$. An observation point $\mathbf{x}$ close to $\mathbf{x}_0$ is written as $\mathbf{x} = \mathbf{x}_0 + \varepsilon\boldsymbol{\xi}$, so that in the new variables

$$\mathbf{u}^B_\varepsilon(\boldsymbol{\xi};\mathbf{x}_0) = \int_{\mathbb{R}^9} \Gamma G^2_\varepsilon(T, \mathbf{x}_0 + \varepsilon\boldsymbol{\xi}; \mathbf{y}) \Gamma G^1_\varepsilon(T, \mathbf{y}'; \mathbf{x}_0 + \varepsilon\mathbf{z}) \times \mathbf{S}(\mathbf{z}) \chi_\Omega(\mathbf{y}) \chi_\Omega(\mathbf{y}') f(\frac{\mathbf{y}-\mathbf{y}'}{\varepsilon}) d\mathbf{y} d\mathbf{y}' d\mathbf{z}.$$

We thus want to understand the limiting properties (as $\varepsilon \to 0$) of the 4×4-matrix $G^2_\varepsilon(T, \mathbf{x}_0 + \varepsilon\boldsymbol{\xi}; \mathbf{y}) \Gamma G^1_\varepsilon(T, \mathbf{y}'; \mathbf{x}_0 + \varepsilon\mathbf{z})$. We use kinetic models for this.

How to use kinetic theories

Recall that the Wigner transform of two fields $\mathbf{u}$ and $\mathbf{v}$ satisfies an equation of the form

$$\varepsilon\frac{\partial W_\varepsilon}{\partial t} + P(i\mathbf{k} + \frac{\varepsilon \mathbf{D}}{2})W_\varepsilon + W_\varepsilon P^*(i\mathbf{k} - \frac{\varepsilon \mathbf{D}}{2}) + \sqrt{\varepsilon}\Big(\mathcal{K}_\varepsilon^1 K W_\varepsilon + \mathcal{K}_\varepsilon^{2*} W_\varepsilon K^*\Big) = 0,$$

which comes from $\mathbf{u}$ and $\mathbf{v}$ solving equations of the form

$$\varepsilon\frac{\partial \mathbf{u}}{\partial t} + B_\varepsilon \mathbf{u} = 0, \qquad \varepsilon\frac{\partial \mathbf{v}^*}{\partial t} + \mathbf{v}^* B_\varepsilon^* = 0,$$

where $\mathbf{v}^* B_\varepsilon^*$ has to be interpreted in the pseudo-differential sense, i.e., as in the inverse Fourier transform of the vector $\hat{\mathbf{v}}^*(t,\mathbf{k})\widehat{B}_\varepsilon(\mathbf{x},\mathbf{k})$, where $\widehat{B}_\varepsilon(\mathbf{x},\mathbf{k})$ is the symbol of $B_\varepsilon(\mathbf{x}, D)$.

To find an equation for the Wigner transform of matrix-valued Green functions, we need a pair similarly satisfying the equations

$$\varepsilon\frac{\partial G_\varepsilon}{\partial t} + B_\varepsilon G_\varepsilon = 0, \qquad \varepsilon\frac{\partial G_\varepsilon^*}{\partial t} + G_\varepsilon^* B_\varepsilon^* = 0.$$

An adjoint Green's matrix

Recall that the Green function $G^1(t,\mathbf{x};\mathbf{y})$ solves the equation

$$A^1\frac{\partial G^1(t,\mathbf{x};\mathbf{y})}{\partial t}+D^j\frac{\partial}{\partial x_j}(G^1(t,\mathbf{x};\mathbf{y}))=0,\qquad G^1(0,\mathbf{x};\mathbf{y})=\delta(\mathbf{x}-\mathbf{y})I.$$

Introduce the adjoint Green's matrix G^1_*, solution of

$$\frac{\partial G^1_*(t,\mathbf{x};\mathbf{y})}{\partial t}+\frac{\partial G^1_*(t,\mathbf{x};\mathbf{y})}{\partial x_j}D^j(A^1)^{-1}(\mathbf{x})=0,\ G^1_*(0,\mathbf{x};\mathbf{y})=\delta(\mathbf{x}-\mathbf{y})\Gamma A^{-1}(\mathbf{y})\Gamma.$$

We verify the following Maxwell reciprocity-type result

$$\Gamma G^1(t,\mathbf{y};\mathbf{x})=G^1_*(t,\mathbf{x};\mathbf{y})A^1(\mathbf{x})\Gamma.$$

This allows us to recast the back-propagated signal as

$$\mathbf{u}^B_\varepsilon(\boldsymbol{\xi};\mathbf{x}_0)=\int_{\mathbb{R}^9}\Gamma G^2_\varepsilon(T,\mathbf{x}_0+\varepsilon\boldsymbol{\xi};\mathbf{y})G^1_{\varepsilon*}(T,\mathbf{x}_0+\varepsilon\mathbf{z};\mathbf{y}')A^1_\varepsilon(\mathbf{x}_0+\varepsilon\mathbf{z})\Gamma$$
$$\times\mathbf{S}(\mathbf{z})\chi_\Omega(\mathbf{y})\chi_\Omega(\mathbf{y}')f(\frac{\mathbf{y}-\mathbf{y}'}{\varepsilon})d\mathbf{y}d\mathbf{y}'d\mathbf{z}.$$

Theory of time-reversal refocusing

Introduce now the Wigner transform

$$W_\varepsilon(t,\mathbf{x},\mathbf{k}) = \int_{\mathbb{R}^6} \Big[\int_{\mathbb{R}^3} e^{i\mathbf{k}\cdot\mathbf{z}} G^2_\varepsilon(t,\mathbf{x}-\frac{\varepsilon\mathbf{z}}{2};\mathbf{y}) G^1_{\varepsilon *}(t,\mathbf{x}+\frac{\varepsilon\mathbf{z}}{2};\mathbf{y}')\frac{d\mathbf{z}}{(2\pi)^3}\Big]$$
$$\times \chi_\Omega(\mathbf{y})\chi_\Omega(\mathbf{y}') f(\frac{\mathbf{y}-\mathbf{y}'}{\varepsilon}) d\mathbf{y} d\mathbf{y}',$$

which satisfies the same equation as we have seen before. This allows us to write the refocused signal in terms of the Wigner transform as

$$\boxed{\mathbf{u}^B_\varepsilon(\boldsymbol{\xi};\mathbf{x}_0) = \int_{\mathbb{R}^6} \Gamma W_\varepsilon(t,\mathbf{x}_0+\varepsilon\frac{\boldsymbol{\xi}+\mathbf{z}}{2},\mathbf{k}) e^{-i\mathbf{k}\cdot(\mathbf{z}-\boldsymbol{\xi})} A^1_\varepsilon(\mathbf{x}_0+\varepsilon\mathbf{z})\Gamma \mathbf{S}(\mathbf{z}) d\mathbf{z} d\mathbf{k}.}$$

High frequency estimates of refocusing are obtained by analyzing the limit of $W_\varepsilon(t,\mathbf{x},\mathbf{k})$ as $\varepsilon\to 0$: $\boxed{\hat{\mathbf{u}}^B(\mathbf{k};\mathbf{x}_0) = \Gamma W_0(t,\mathbf{x}_0,\mathbf{k}) A^1_0(\mathbf{x}_0)\Gamma\hat{\mathbf{S}}(\mathbf{k})}$.

Kinetic theory in weak coupling regime

The Wigner distribution at time $t = 0$ is given by

$$W(0, \mathbf{x}, \mathbf{k}) = |\chi_\Omega(\mathbf{x})|^2 \hat{f}(\mathbf{k}) A_0^{-1}(\mathbf{x}), \text{ where } (A_\varepsilon^\varphi)^{-1} = A_0^{-1} + O(\sqrt{\varepsilon}).$$

The limit Wigner distribution is decomposed as:
$W(t, \mathbf{x}, \mathbf{k}) = a_+(t, \mathbf{x}, \mathbf{k})\mathbf{b}_+\mathbf{b}_+^* + a_-(t, \mathbf{x}, \mathbf{k})\mathbf{b}_-\mathbf{b}_-^*$. Furthermore, the **radiative transfer equation** for a_+ is (with $\omega_+ = -c_0|\mathbf{k}|$)

$$\begin{aligned}
\frac{\partial a_+}{\partial t} + c_0 \hat{\mathbf{k}} \cdot \nabla a_+ + (\Sigma(\mathbf{k}) + i\Pi(\mathbf{k}))a_+ & \\
= \frac{\pi \omega_+^2(\mathbf{k})}{2(2\pi)^d} \int_{\mathbb{R}^d} \hat{R}^{12}(\mathbf{k} - \mathbf{q}) a_+(\mathbf{q}) \delta\Big(\omega_+(\mathbf{q}) - \omega_+(\mathbf{k})\Big) d\mathbf{q}, & \\
\Sigma(\mathbf{k}) = \frac{\pi \omega_+^2(\mathbf{k})}{2(2\pi)^d} \int_{\mathbb{R}^d} \frac{\hat{R}^{11} + \hat{R}^{22}}{2}(\mathbf{k} - \mathbf{q}) \delta\Big(\omega_+(\mathbf{q}) - \omega_+(\mathbf{k})\Big) d\mathbf{q} & \\
i\Pi(\mathbf{k}) = \frac{-i\pi \sum_{j=\pm}}{4(2\pi)^d} \text{ p.v.} \int_{\mathbb{R}^d} \Big(\hat{R}^{11} - \hat{R}^{22}\Big)(\mathbf{k} - \mathbf{q}) \frac{\omega_j(\mathbf{k})\omega_+(\mathbf{q})}{\omega_j(\mathbf{q}) - \omega_+(\mathbf{k})} d\mathbf{q}. &
\end{aligned}$$

Robustness of Time Reversal

The refocusing is extremely sensitive to modifications in the “random” medium. It is however very robust when other operations than time reversal are performed at the receivers.

Let us assume that the usual time reversal operation represented by $\Gamma_0 = \mathrm{Diag}(-1,-1,-1,1)$ is replaced by multiplication by an (almost) arbitrary $\Gamma(\mathbf{x})$. The initial conditions for the Wigner transform are then

$$W(0,\mathbf{x},\mathbf{k}) = |\chi(\mathbf{x})|^2\Gamma(\mathbf{x})\Gamma_0 A^{-1}(\mathbf{x})\widehat{f}(\mathbf{k}).$$

The rest of the theory stays unchanged.

Robustness of Time Reversal (II)

The initial conditions for the acoustic modes are then

$$a_{\pm}(0,\mathbf{x},\mathbf{k}) = |\chi(\mathbf{x})|^2 \hat{f}(\mathbf{k})\Big(A(\mathbf{x})\Gamma(\mathbf{x})\mathbf{b}_{\mp}(\mathbf{x},\mathbf{k})\cdot\mathbf{b}_{\pm}(\mathbf{x},\mathbf{k})\Big).$$

When $\Gamma(\mathbf{x}) = \Gamma_0$ we get back full time reversal results. When $\Gamma = Id$, we obtain that $a_{\pm}(0,\mathbf{x},\mathbf{k}) = 0$ by orthogonality of the eigenvectors $\mathbf{b}_j$. When only pressure is measured, $\Gamma = \mathrm{Diag}(0,0,0,1)$, we obtain

$$a_{\pm}(0,\mathbf{x},\mathbf{k}) = \frac{1}{2}|\chi(\mathbf{x})|^2 \hat{f}(\mathbf{k}).$$

When only the first component of the velocity field is measured with $\Gamma = \mathrm{Diag}(-1,0,0,0)$, the initial data is

$$a_{\pm}(0,\mathbf{x},\mathbf{k}) = |\chi(\mathbf{x})|^2 \hat{f}(\mathbf{k})\frac{k_1^2}{2|\mathbf{k}|^2}.$$

Outline for Lecture II.

1. Time Reversal in random media

2. Statistical stability

3. Validity of Radiative Transfer Models

4. Applications to Detection and Imaging

Statistical stability in Time Reversal

We saw that there were few theoretical results in the weak coupling regime for the wave equation and they are concerned with ensemble averages of the Wigner transform, not its limiting law.

However such limiting laws are accessible for simplifed regimes of radiative transfer, including paraxial approximations, Itô-Schrödinger approximations, and random Liouville equations.

Such limiting laws directly translate into results on the statistical stability of the time reversed signals whether the underlying media change or not between the two stages of the time reversal experiment.

Main stability result in paraxial approximation

Theorem. Let the array $\chi(\mathbf{y})$ and the *filter* $f(\mathbf{y})$ *be in* $L^1 \cap L^\infty(\mathbb{R}^d)$, while $\psi_0 \in L^2(\mathbb{R}^d)$ for a given $\kappa \in \mathbb{R}$. Then for each $\boldsymbol{\xi} \in \mathbb{R}^d$ the back-propagated signal $\psi_\varepsilon^B(\boldsymbol{\xi}, \mathbf{x}_0, \kappa)$ converges in probability and weakly in $L^2_{\mathbf{x}_0}(\mathbb{R}^d)$ as $\varepsilon \to 0$ to the deterministic

$$\psi^B(\boldsymbol{\xi}, \kappa; \mathbf{x}_0) = \int_{\mathbb{R}^{2d}} e^{i\mathbf{k}\cdot(\boldsymbol{\xi}-\mathbf{y})} \overline{W}(L, \mathbf{x}_0, \mathbf{k}, \kappa) \psi_0(\mathbf{y}, \kappa) \frac{d\mathbf{y}\, d\mathbf{k}}{(2\pi)^d}.$$

The function $\overline{W}$ satisfies the transport equation

$$\frac{\partial \overline{W}}{\partial z} + \frac{1}{\kappa} \mathbf{k} \cdot \nabla_{\mathbf{x}} \overline{W} = \kappa \mathcal{L} \overline{W},$$

with initial data $\overline{W}_0(\mathbf{x}, \mathbf{k}) = \hat{f}(\mathbf{k}) |\chi(\mathbf{x})|^2$ and operator $\mathcal{L}$ defined by

$$\mathcal{L}\lambda = \int_{\mathbb{R}^d} \frac{d\mathbf{p}}{(2\pi)^d} \hat{R}\left(\frac{|\mathbf{p}|^2 - |\mathbf{k}|^2}{2}, \mathbf{p} - \mathbf{k}\right)(\lambda(\mathbf{p}) - \lambda(\mathbf{k})),$$

where $\hat{R}(\omega, \mathbf{p})$ is the Fourier transform of the correlation function of V.

Stability of TR in Itô-Schrödinger regime

Theorem. Assume that the initial condition $\psi_0(\mathbf{y}) \in L^2(\mathbb{R}^d)$, the filter $f(\mathbf{y}) \in L^1(\mathbb{R}^d) \cap L^2(\mathbb{R}^d)$, and the detector amplification $\chi(\mathbf{x})$ is sufficiently smooth. Then $\psi^B_\eta(\boldsymbol{\xi}; \mathbf{x}_0)$ converges weakly and in probability as $\eta \to 0$ to the deterministic *back-propagated signal*

$$\psi^B(\boldsymbol{\xi}; \mathbf{x}_0) = \int_{\mathbb{R}^d} e^{i\mathbf{k}\cdot\boldsymbol{\xi}} \overline{W}(\mathbf{x}_0, \mathbf{k}, L) \hat{\psi}_0(\mathbf{k}) d\mathbf{k},$$

where $\overline{W}(\mathbf{x}_0, \mathbf{k}, L)$ is the solution of a RTE with initial conditions $\overline{W}(\mathbf{x}, \mathbf{k}, 0) = \hat{f}(\mathbf{k})|\chi(\mathbf{x})|^2$. Moreover introducing $\lambda(\boldsymbol{\xi}, \mathbf{x}_0) = \tilde{\lambda}(\mathbf{x}_0)\mu(\boldsymbol{\xi})$ we have the following estimate

$$\left\langle (\psi^B_\eta - \langle \psi^B_\eta \rangle, \lambda)^2 \right\rangle \leq C\eta^d \|\psi_0\|_2^2 \|\lambda\|_2^2 = C\eta^d \|\psi_0\|_2^2 \|\mu\|_2^2 \|\tilde{\lambda}\|_2^2,$$

uniformly in L on compact intervals.

We *do not* have such an estimate for the *parabolic* approximation and the test function is allowed to have much smaller support.

Stability of TR in random Liouville regime

Theorem. The re-propagated field $\mathbf{v}_\varepsilon^{\delta,B}(\boldsymbol{\xi},\mathbf{x}_0)$ converges as $(\varepsilon,\delta)\to 0$

$$\mathbf{v}^B(\boldsymbol{\xi},\mathbf{x}_0)=\int e^{i\mathbf{k}\cdot\boldsymbol{\xi}}\Big[\;u_+(T,\mathbf{x}_0,\mathbf{k})\langle\widehat{S}_0(\mathbf{k}),\mathbf{b}_-(\mathbf{k})\rangle\mathbf{b}_+(\mathbf{k}) + u_-(T,\mathbf{x}_0,\mathbf{k})\langle\widehat{S}_0(\mathbf{k}),\mathbf{b}_+(\mathbf{k})\rangle\mathbf{b}_-(\mathbf{k})\Big]\frac{d\mathbf{k}}{(2\pi)^d}$$

in the sense that

$$\sup_{\boldsymbol{\xi}\in\mathbb{R}^d}\mathbb{E}\left\{\int|\mathbf{v}_\varepsilon^{\delta,B}(\boldsymbol{\xi},\mathbf{x}_0)-\mathbf{v}^B(\boldsymbol{\xi},\mathbf{x}_0)|^2d\mathbf{x}_0\right\}\to 0.$$

The functions $u_\pm(t,\mathbf{x},\mathbf{k})$ are the solutions of the Fokker-Planck equation

$$\frac{\partial\bar{u}_\pm}{\partial t}\pm c_0\hat{\mathbf{k}}\cdot\nabla_{\mathbf{x}}\bar{u}_\pm=\frac{\partial}{\partial k_m}\left[|\mathbf{k}|^2D_{mn}(\hat{\mathbf{k}})\frac{\partial\bar{u}_\pm}{\partial k_n}\right],\qquad u_\pm(0,\mathbf{x},\mathbf{k})=|\chi(\mathbf{x})|^2\hat{f}(\mathbf{k}),$$

where

$$D_{mn}=\frac{1}{2}\int_{-\infty}^{\infty}\frac{\partial^2R(c_0s\hat{\mathbf{k}})}{\partial x_n\partial x_m}ds,\qquad\mathbb{E}\left\{c_1(\mathbf{y})c_1(\mathbf{x}+\mathbf{y})\right\}=R(\mathbf{x}).$$

Outline for Lecture II.

1. Time Reversal in random media

2. Statistical stability

3. **Validity of Radiative Transfer Models**

4. Applications to Detection and Imaging

Time reversal in changing media

Consider two media such that the compressibility fluctuations are given by $\hat{\kappa}_2(\mathbf{x},\mathbf{k}) = \phi(\mathbf{x}) e^{i\boldsymbol{\tau}\cdot\mathbf{k}} \hat{\kappa}_1(\mathbf{x},\mathbf{k})$. For instance $\phi(\mathbf{x})$ corresponds to a change in the amplitude of the fluctuations at the macroscopic scale $\mathbf{x}$ and $\boldsymbol{\tau}$ corresponds to a spatial shift in the domain before back-propagation. Then the propagating modes satisfy

$$\frac{\partial a_\pm}{\partial t} \pm c_0 \hat{\mathbf{k}} \cdot \nabla a_\pm + \Big(\sigma_a(\mathbf{k}) \pm i\Pi(\mathbf{k})\Big) a_\pm = Q a_\pm,$$
$$a_\pm(0,\mathbf{x},\mathbf{k}) = |\chi(\mathbf{x})|^2$$

$$Qa(\mathbf{k}) = \int_{\mathbb{R}^3} \sigma(\mathbf{k},\mathbf{p}) \phi(\mathbf{x},\mathbf{p}-\mathbf{k}) \Big(a(\mathbf{p}) - a(\mathbf{k})\Big) \delta(c_0(|\mathbf{k}|-|\mathbf{p}|)) d\mathbf{p}$$
$$\Pi(\mathbf{k}) = \fint_{\mathbb{R}^3} (1 - |\phi(\mathbf{x},\mathbf{p}-\mathbf{k})|^2) \frac{c_0}{2} \frac{|\mathbf{k}||\mathbf{p}|^2}{|\mathbf{k}|^2 - |\mathbf{p}|^2} \frac{\hat{R}(\mathbf{k}-\mathbf{p})}{(2\pi)^3} d\mathbf{p}$$
$$\sigma_a(\mathbf{k}) = \int_{\mathbb{R}^3} \sigma(\mathbf{k},\mathbf{p}) \Big(\frac{1 + |\phi(\mathbf{x},\mathbf{p}-\mathbf{k})|^2}{2} - \phi(\mathbf{x},\mathbf{p}-\mathbf{k})\Big) \delta(c_0(|\mathbf{k}|-|\mathbf{p}|)) d\mathbf{p}.$$

Diffusion Approximation

Assume $\Sigma = O(\eta^{-1})$, $\sigma_a = O(\eta)$, and $|\phi| = (1+\eta\psi)$. Use $a = a_0 + \eta a_1 + \eta^2 a_2$, plug Ansatz into transport equation, equate like powers of η and deduce that a_0 solves the following diffusion equation:

$$\frac{\partial a_0}{\partial t} + \frac{\Sigma(|\mathbf{k}|)\psi^2}{2} a_0 - D(|\mathbf{k}|)\Delta a_0 = 0,$$
$$e^{-i\Pi(|\mathbf{k}|)t/\eta^2} a_0(0,\mathbf{x}) = |\chi(\mathbf{x})|^2 \frac{1}{4\pi}\int_{S^2} e^{i\boldsymbol{\tau}\cdot\mathbf{k}} d\hat{\mathbf{k}} = |\chi(\mathbf{x})|^2 \frac{\sin|\boldsymbol{\tau}||\mathbf{k}|}{|\boldsymbol{\tau}||\mathbf{k}|}$$

$$D(|\mathbf{k}|) = \frac{c_0^2}{3[\Sigma(|\mathbf{k}|) - \lambda(|\mathbf{k}|)]} = \frac{c_0\, l^*}{3} = \frac{c_0\, l}{3\Big(1 - \frac{\lambda(|\mathbf{k}|)}{\Sigma(|\mathbf{k}|)}\Big)}$$
$$\lambda(|\mathbf{k}|)\hat{\mathbf{k}} = \frac{c_0^2|\mathbf{k}|^2}{(4\pi)^2}\int_{\mathbb{R}^3} \hat{R}(\mathbf{p}-\mathbf{k})\hat{\mathbf{p}}\delta(c_0(|\mathbf{k}|-|\mathbf{p}|))d\mathbf{p}.$$

Application to Filters in Time Reversal

The back-propagated signal in the diffusive regime takes the form

$$\hat{\mathbf{u}}^B(\mathbf{k};\mathbf{x}_0) = \left[\begin{pmatrix} \sin(\Pi_s T)\sqrt{\dfrac{\kappa_0}{\rho}} i\hat{\mathbf{k}} \\ \cos(\Pi_s T) \end{pmatrix} \hat{p}_0(\mathbf{k}) + \begin{pmatrix} \cos(\Pi_s T) i\hat{\mathbf{k}} \\ -\sin(\Pi_s T)\sqrt{\dfrac{\rho}{\kappa_0}} \end{pmatrix} |\mathbf{k}|\hat{\varphi}(\mathbf{k}) \right] \\ \times e^{-i\boldsymbol{\tau}\cdot\mathbf{k}} \; \frac{\sin|\boldsymbol{\tau}||\mathbf{k}|}{|\boldsymbol{\tau}||\mathbf{k}|} \; e^{-\Sigma\psi^2 T/2} \; a(T,\mathbf{x}_0,|\mathbf{k}|).$$

This is to be compared to the case where $\Pi_s = \psi = |\boldsymbol{\tau}| = 0$ when the medium remains the same during the forward and backward propagations.

2D Numerical simulations

In two space dimensions and in the case of periodic media with distances of propagation large compared to the size of the box, the filter is asymptotically given by

$$F(\psi, |\boldsymbol{\tau}|, |\mathbf{k}|, T, L, k_{\text{max}}, \kappa) = \bar{a}\, J_0(|\boldsymbol{\tau}||\mathbf{k}|)\ \cos(2\psi \Pi_0 T)\, e^{-\frac{\Sigma}{2}\psi^2 T}.$$

It should be compared to the numerical simulation

$$F_{\text{data}} = \frac{(p^B(\mathbf{x}+\boldsymbol{\tau}), p_0(\mathbf{x}))}{\|p_0(\mathbf{x})\|^2}.$$

We consider some simulations with varying $|\boldsymbol{\tau}|$ (shifting medium).

2D Numerical simulations (II)

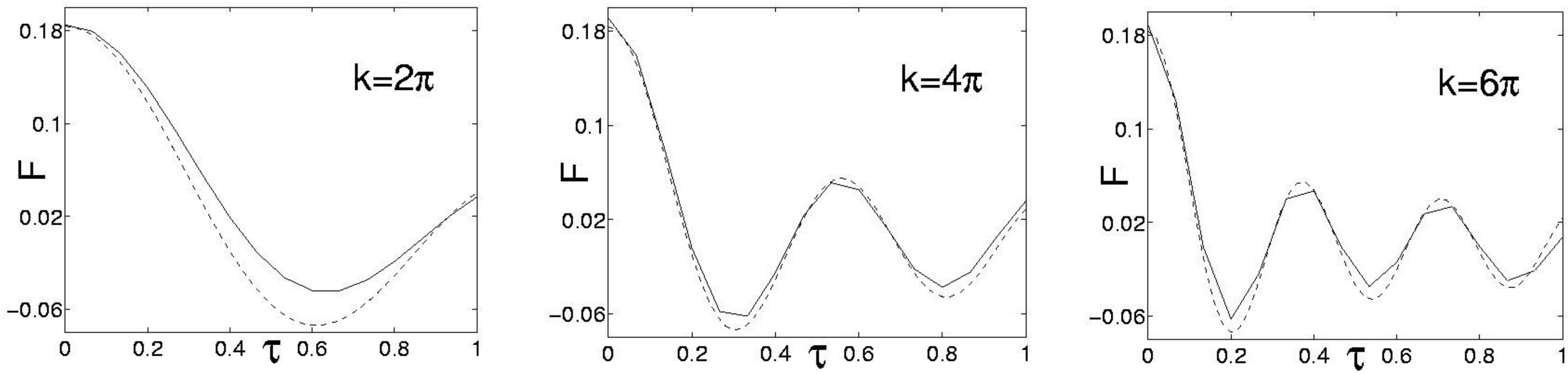

Comparison of F_{data} (solid lines) and the theoretical prediction F (dashed lines) as a function of τ with $\psi = 0$. Periodic box of size $L = 20$, propagation time $T = 200$, number of modes in power spectrum: 50.

Duke experimental setting

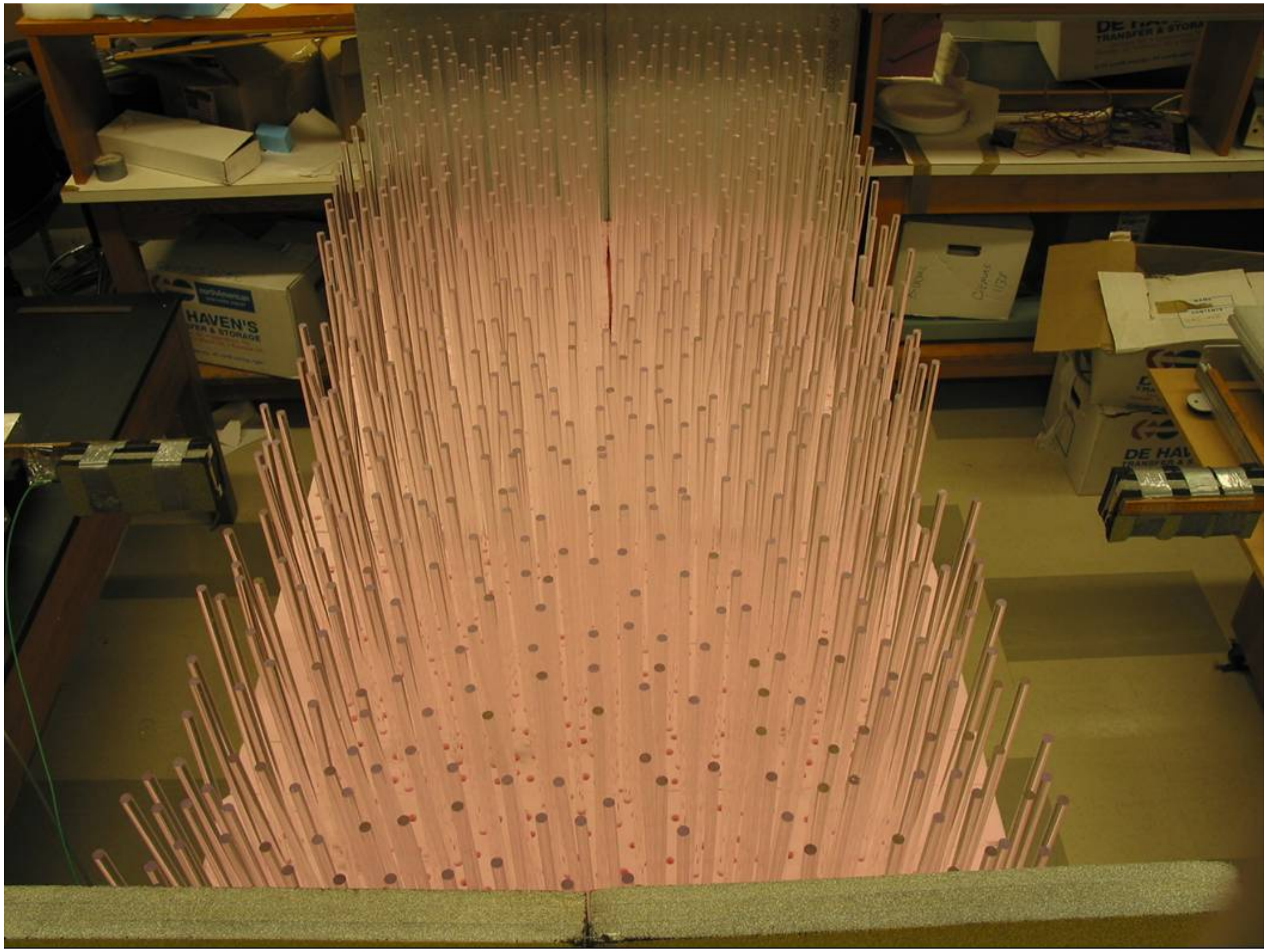

Spatial shift before backpropagation

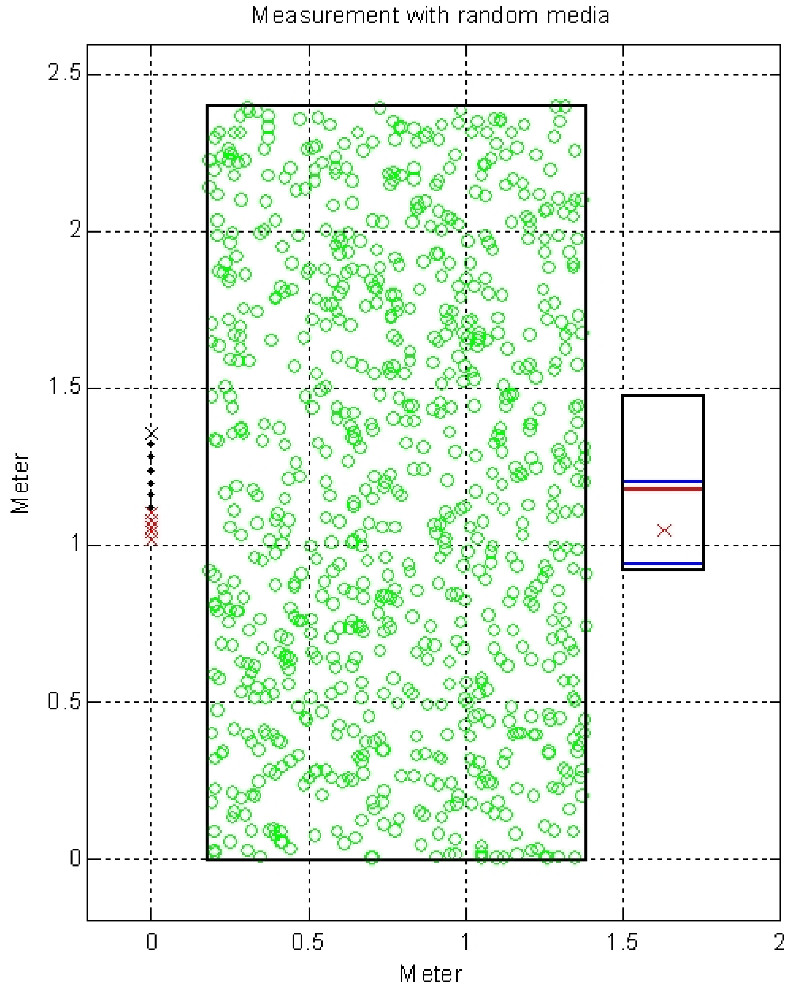

Back-propagated signal

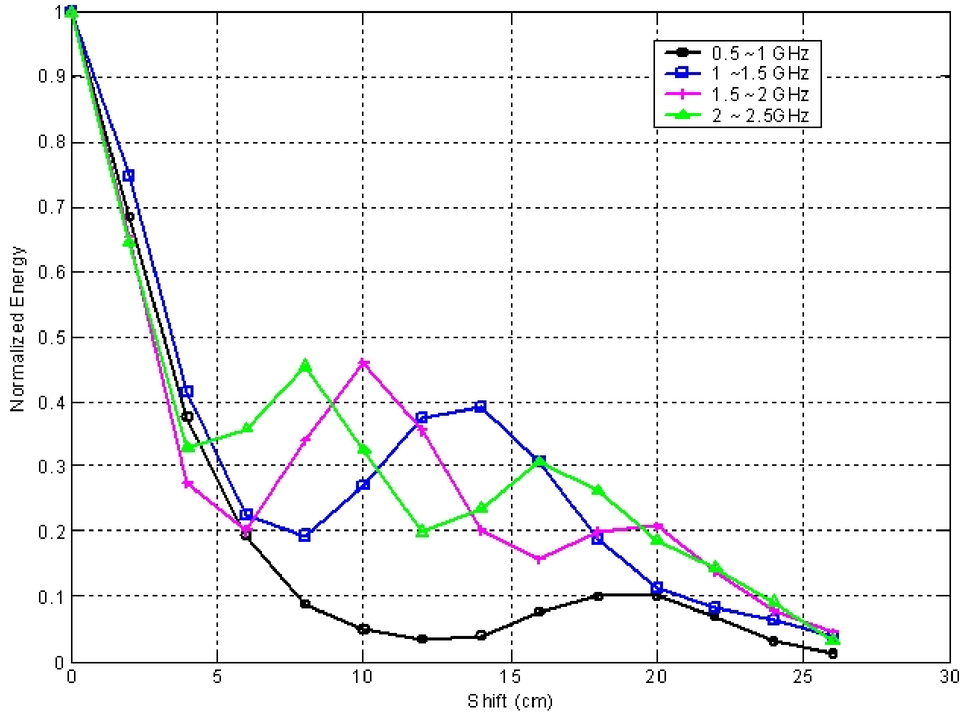

Back-propgated signal as a function of spatial shift for several frequencies. The minimum of the back-propagated signal exactly occurs where it is predicted by the two-dimensional theory.

Numerical validation of radiative transfer

Wave propagation in heterogeneous media may sometimes be difficult to control in real experiments. Numerical simulations offer an interesting complement to physical experiments.

In order to be relevant the simulations need to simulate spatial domains that are much larger than the typical wavelength in the system. This requires us to use multi-processor architectures and parallelized codes.

We have developed such a computational tool to solve acoustic waves (easily extendible to micro-waves) in the time domain, as required by the time reversal framework.

Details of the wave (microscopic) code.

The codes solves a discrete version (centered second-order discretization in space and time) of the following acoustic wave system of equation

$$\frac{\partial \mathbf{v}}{\partial t} + \rho^{-1}(\mathbf{x})\nabla p = 0,$$
$$\frac{\partial p}{\partial t} + \kappa^{-1}(\mathbf{x})\nabla \cdot \mathbf{v} = 0.$$

The domain is surrounded by a perfectly matched layer (PML) method so that outgoing waves are not reflected at the domain boundary. The (random) physical coefficients $\rho(\mathbf{x})$ and $\kappa(\mathbf{x})$ are carefully chosen to verify prescribed statistical properties.

The FDFT (Finite difference forward in time) method has been parallelized by using the software PETSc developed at Argonne. Forward calculations for $T = 1500$ (typical times necessary to validate the diffusive model; for $\lambda = 1$ and average sound speed $c_0 = 1$) require 3-4 days of calculations.

Details of the macroscopic codes.

In both the direct and time reversal measurements, the data are the macroscopic energy densities

$$\mathcal{E}(t,\mathbf{x}) = \frac{1}{2}\Big(\rho(\mathbf{x})|\mathbf{v}|^2(t,\mathbf{x}) + \kappa(\mathbf{x})p^2(t,\mathbf{x})\Big).$$

We consider two macroscopic models for $\mathcal{E}$: a radiative transfer equation and a diffusion equation. The radiative transfer equation is solved by a Monte Carlo method (requiring in excess of $50M$ particles to achieve a reasonable accuracy even with good variance reduction technique conditioning particles on hitting the inclusion). The diffusion equation is solved by the finite element method.

A typical configuration for the wave solver

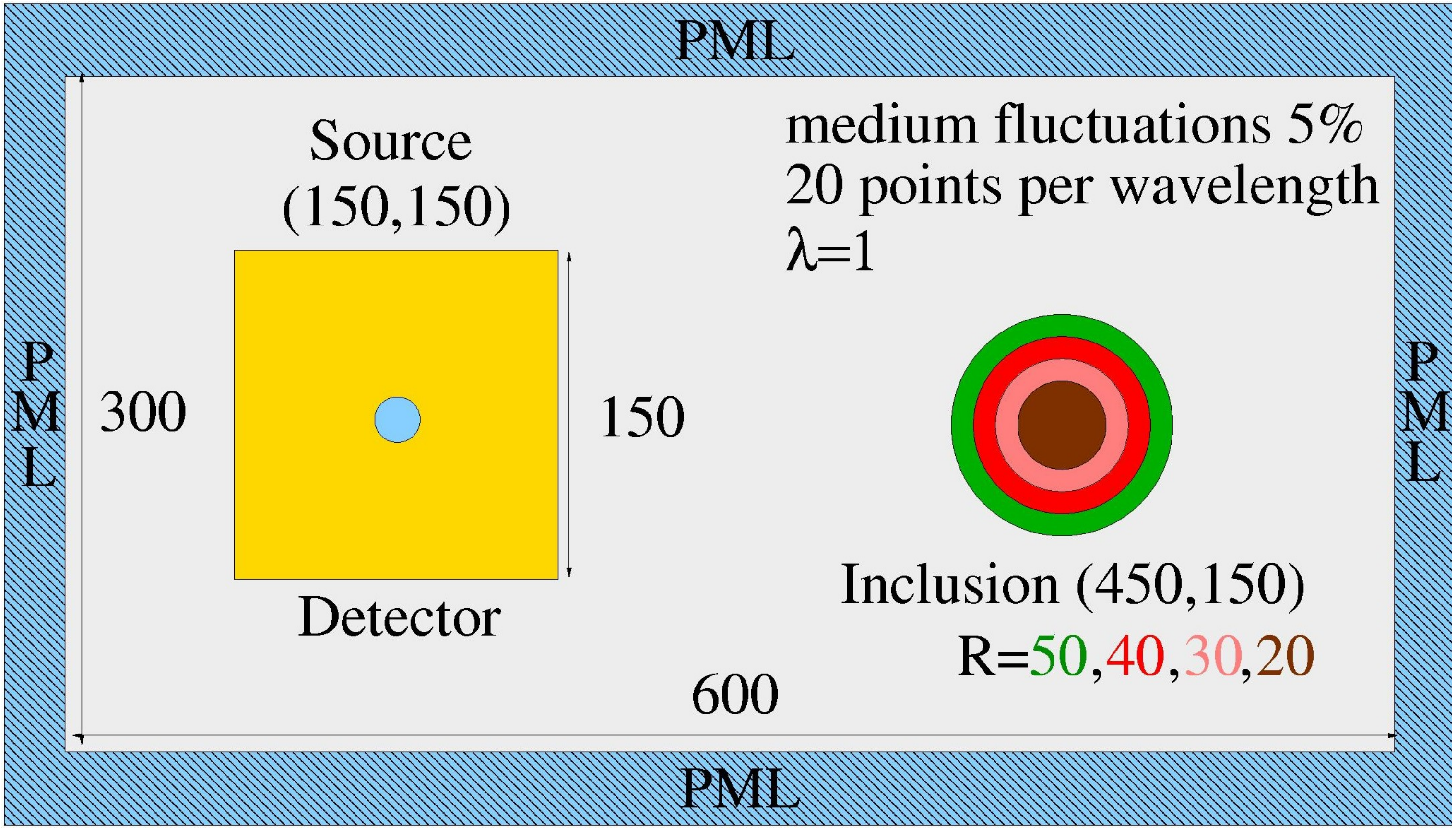

The domain size is roughly $20,000 \times 10,000 = 200M$ nodes

Wave-Transport-diffusion comparison

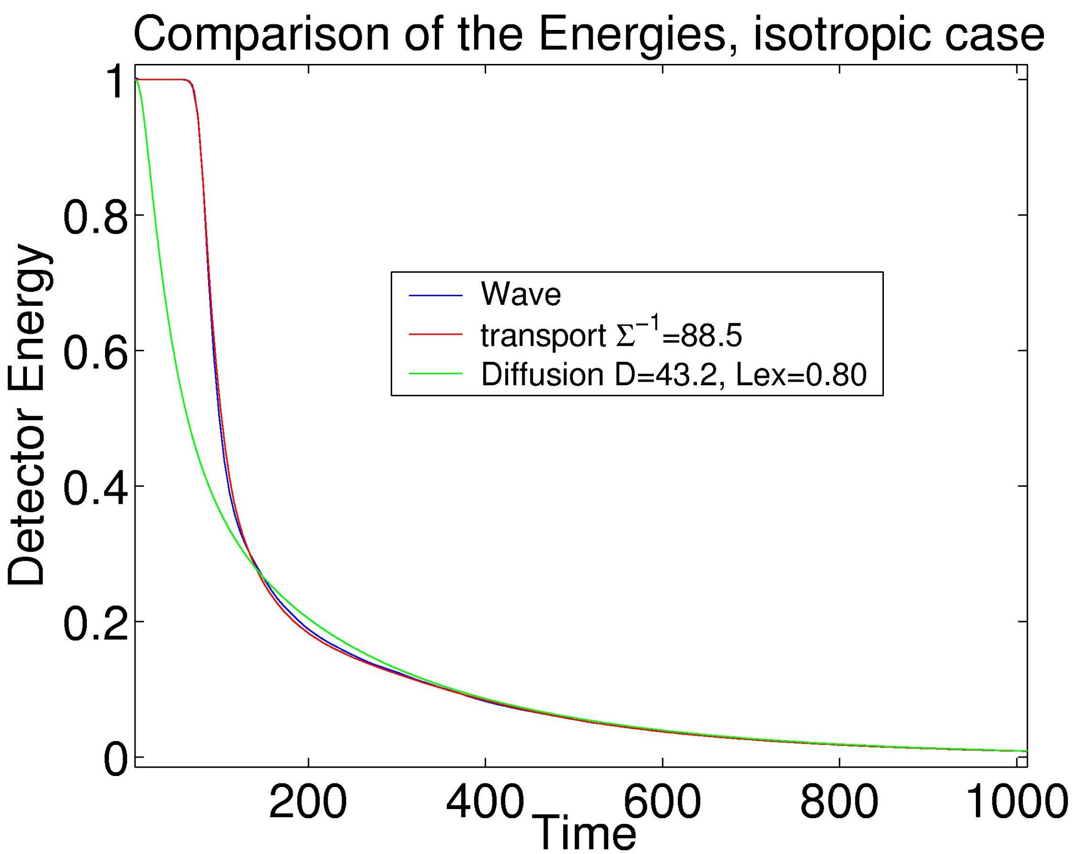

Experiment with isotropic scattering ($\hat{R} \equiv 1$ for this frequency; the source term is a localized Bessel function). The best transport fit is obtained for $\Sigma_{\text{num}}^{-1} = 88.5$ versus $\Sigma_{\text{th}}^{-1} = 83.00$. The best fit for the diffusion coefficient and the extrapolation length are $D_{\text{num}} = 43.2$ and $L_{\text{ex}} = 0.80$ versus $D_{\text{th}} = (2\Sigma)^{-1} = 41.5$ and $L_{\text{th}} = 0.81$.

Averaged energy densities on detector as a function of time.

Effect of void inclusion

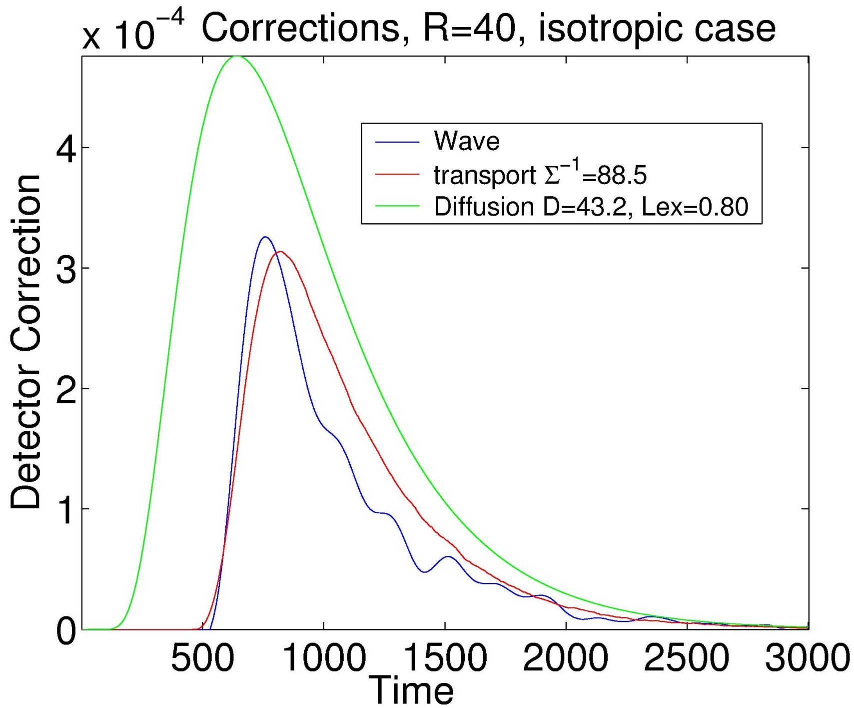

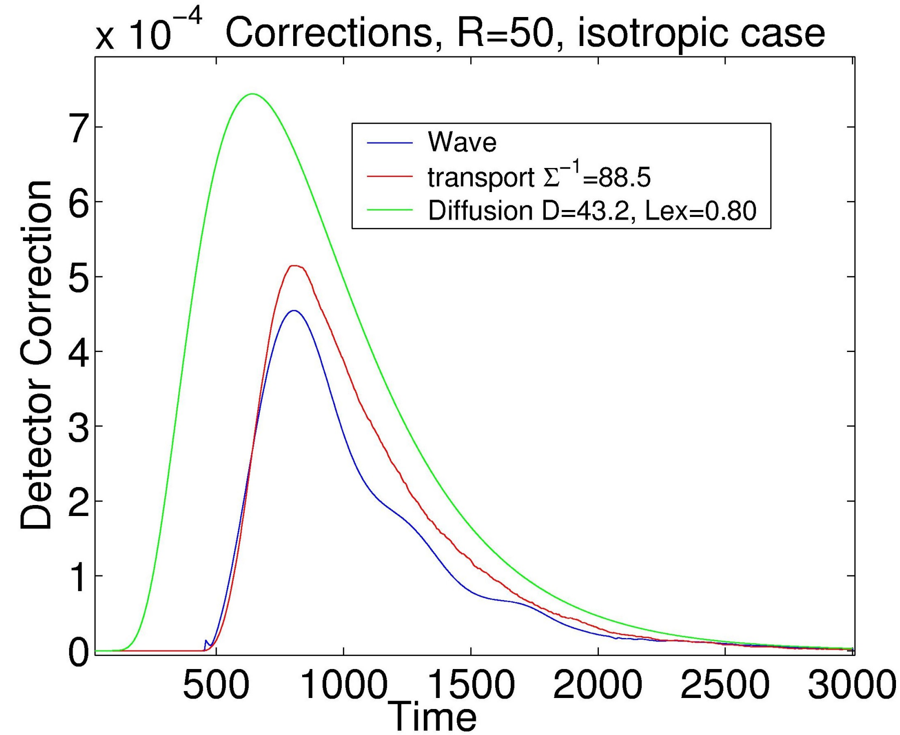

Correction (w.r.t. solution without inclusion) generated by a void inclusion, where the random fluctuations are suppressed. Left, radius of 40. Right, radius of 50. Transport and diffusion generated by best energy fit. The diffusion fit is valid only for very long times, whereas transport performs extremely well.

Effect of increased randomness

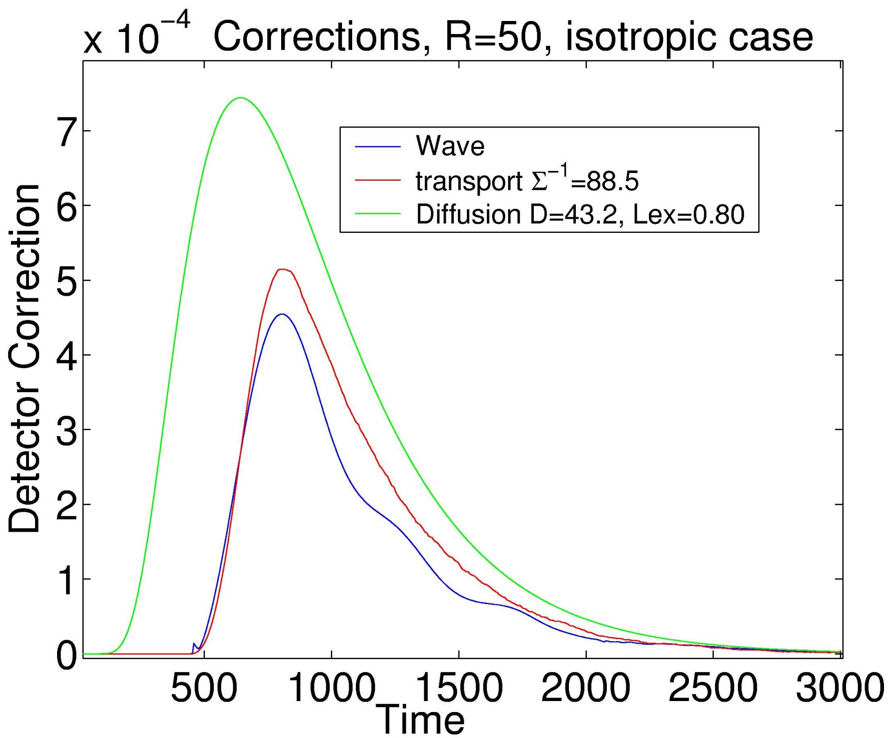

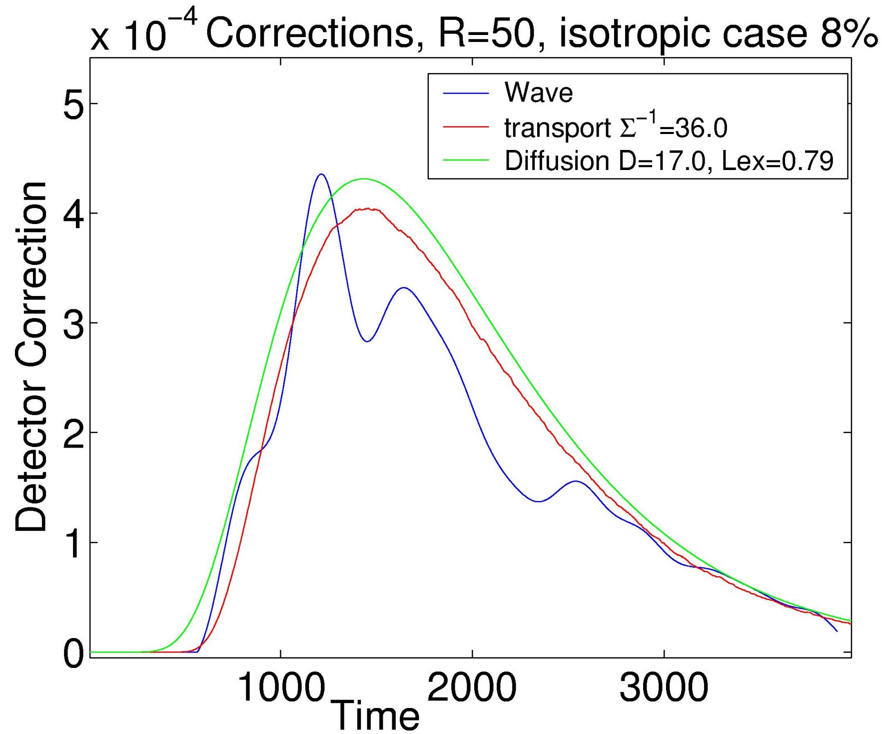

Correction generated by an inclusion of radius $R = 50$ where the random fluctuations are suppressed. Left: 5% RMS. Right: 8% RMS. Transport and diffusion generated by best energy fit. The diffusion fit is now much more accurate.

Effect of perfectly reflecting inclusion

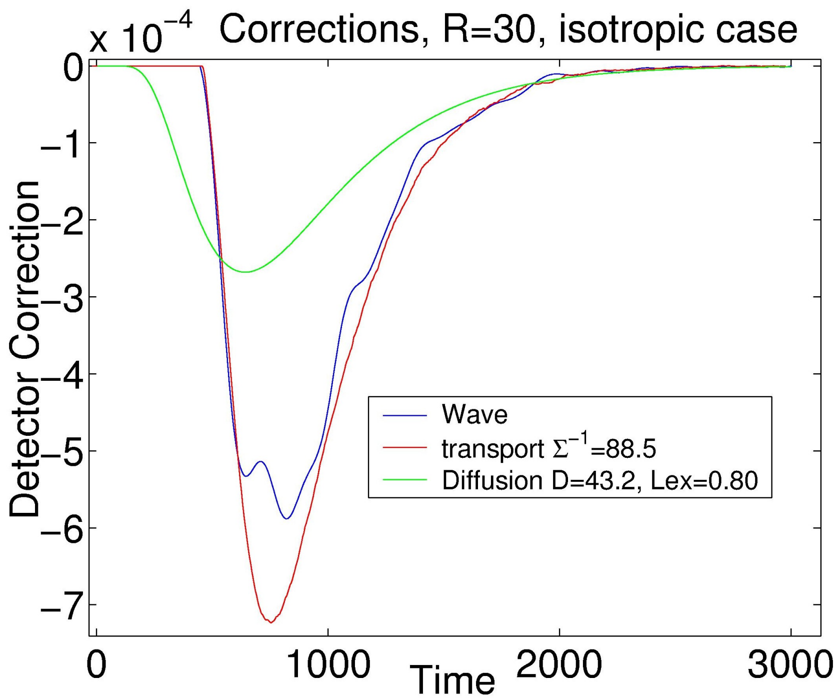

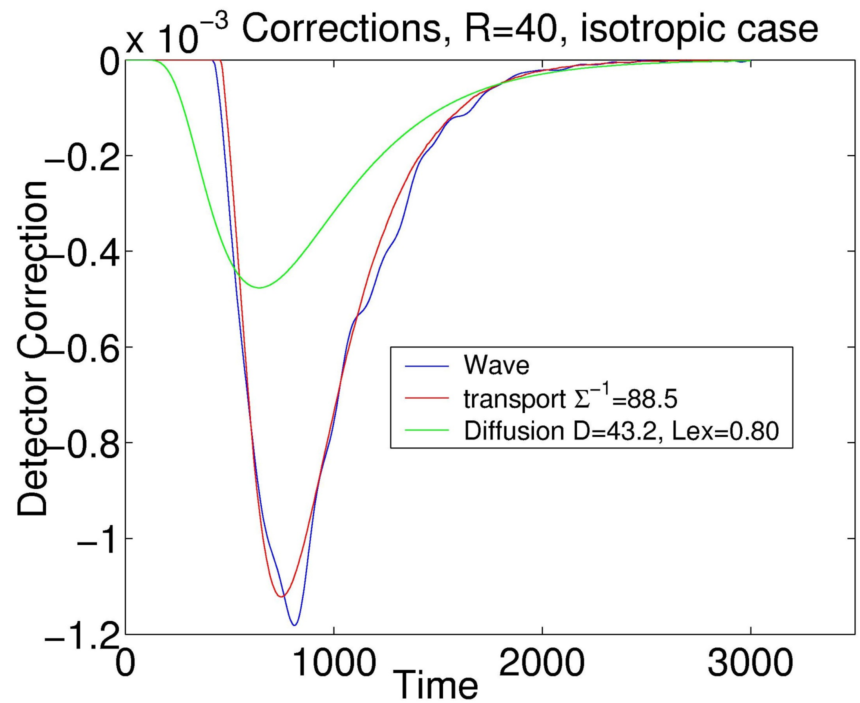

Correction generated by a perfectly reflecting inclusion (specular reflection for transport and Neumann conditions for diffusion). Left, radius of 30. Right, radius of 40. Transport and diffusion generated by best energy fit. Still very good agreement between wave and transport simulations.

Statistical stability

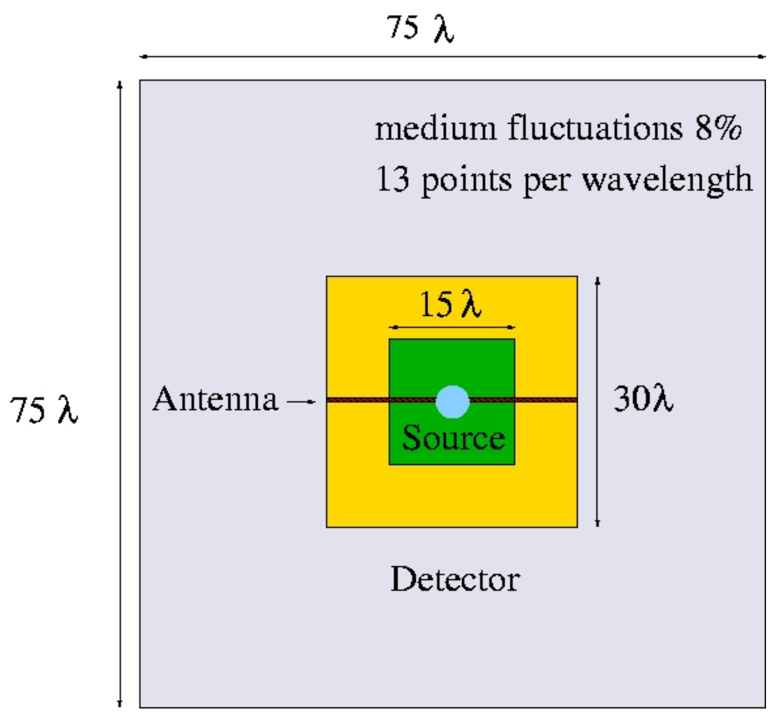

Statistical stability increases when: (i) the power spectrum of the heterogeneities decreases for a given diffusion coefficient (i.e., the same scattering occurs over larger distances); (ii) more independent measurements are taken, for instance by considering moments of the TR filter.

	Bessel			Cosine		
Detection	30×30	15×15	Antenna	30×30	15×15	Antenna
STD (%)	4.6	6.8	4.6	5.9	6.6	6.1

Stability of angularly averaged (Bessel) and angularly dependent (Cosine) filters for different spatial detectors in above configuration.

Outline for Lecture II.

1. Time Reversal in random media

2. Statistical stability

3. Validity of Radiative Transfer Models

4. **Applications to Detection and Imaging**

Experimental setting; forward stage

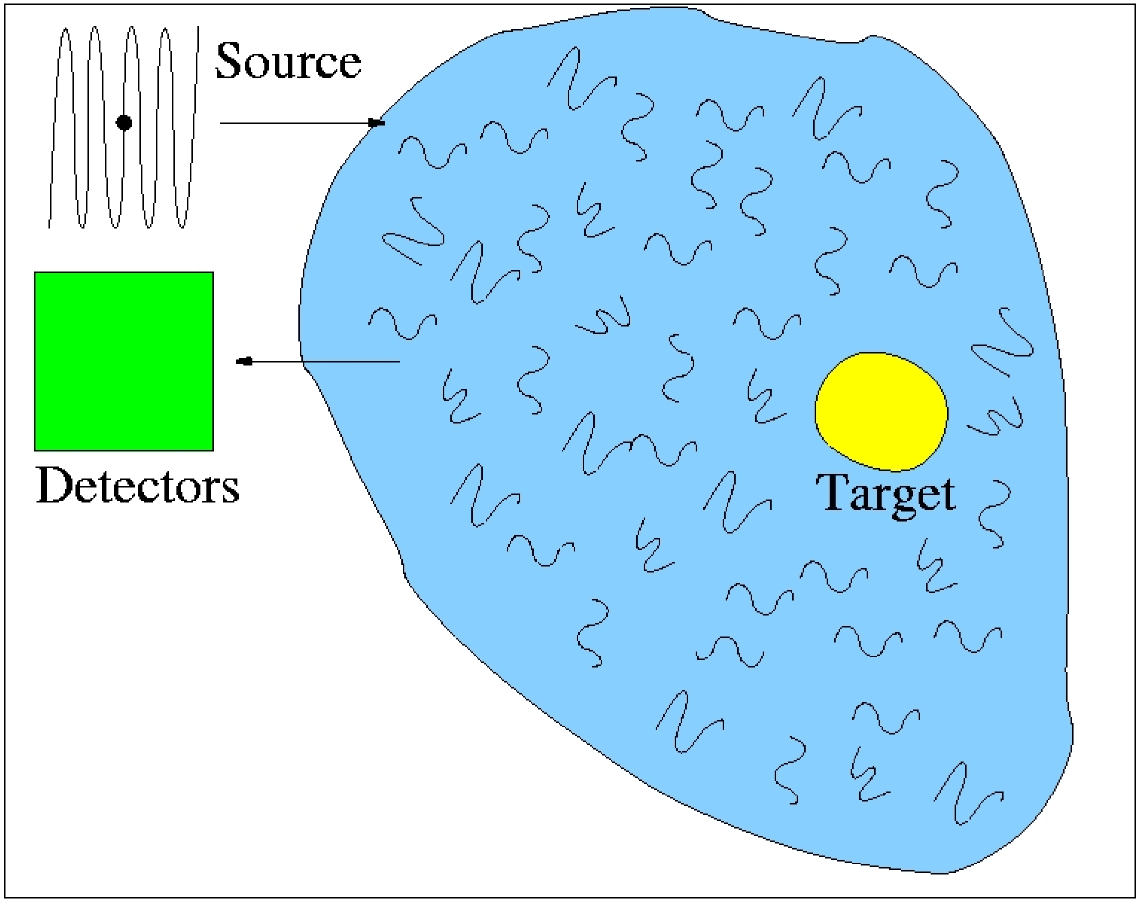

Experimental setting; backward stage

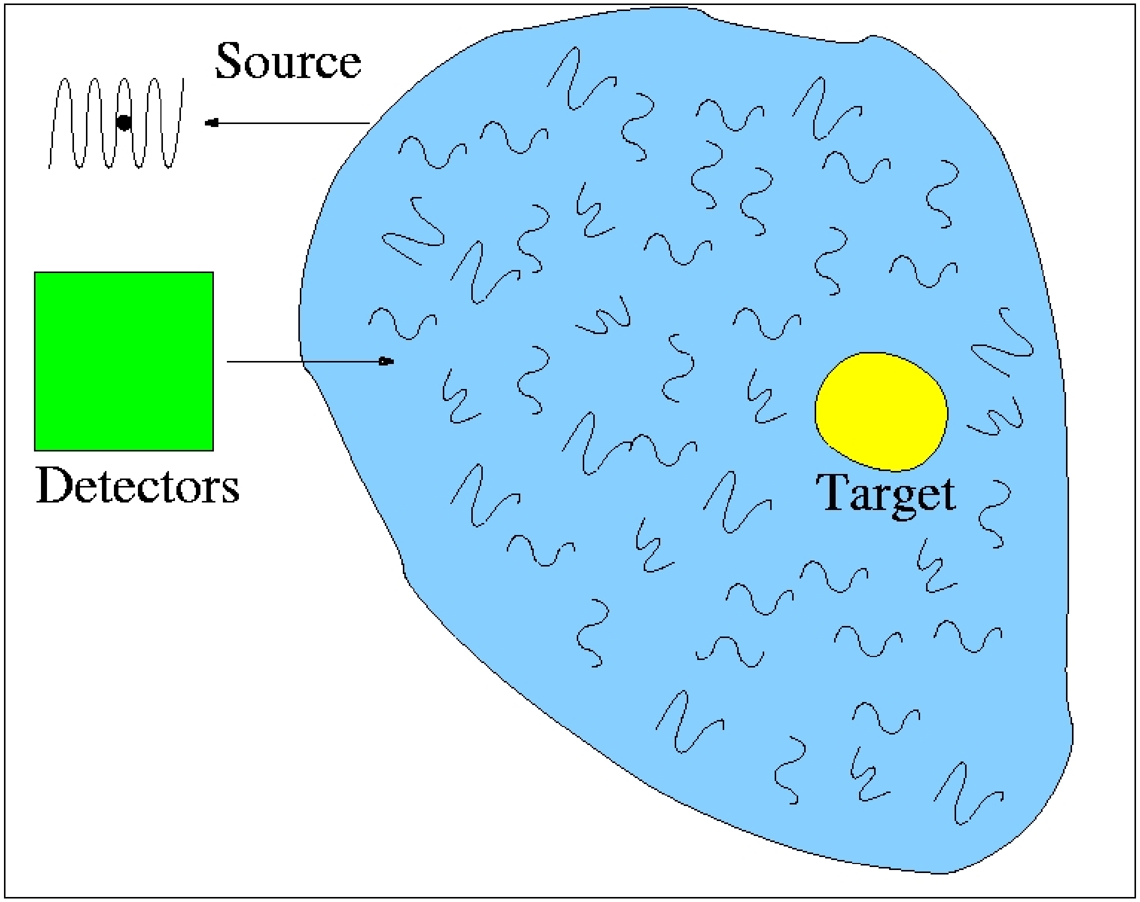

Modeling the inclusion

The detection and imaging of buried inclusions (which are large compared to the wavelength) is done as follows. We model the inclusion as a variation in the kinetic parameters of the radiative transfer equation that models the wave energy density.

The objective is to reconstruct these kinetic parameters from wave energy measurements at the boundary of a domain. This is severely ill-posed problem (in the sense that the reconstruction amplifies noise drastically). Because the inclusion is assumed to be of small volume (at the macroscopic scale), further assumptions are possible. We consider asymptotics in the volume of the inclusion, which take the form

$$\delta a^0(t,\mathbf{x},\mathbf{k}) = -|B| \int_0^t G(t-s,\mathbf{x},\mathbf{x}_b,\mathbf{k})\,(Qa^0)(s,\mathbf{x}_b,\mathbf{k})ds + \text{l.o.t.},$$

where a^0 is the unperturbed solution, G the transport Green's function, Q the scattering operator and $|B| \sim R^d$ the inclusion's volume.

Reconstruction of the inclusion

Detection and imaging based on the above asymptotic expansions allow us obtain the inclusion's location and volume:

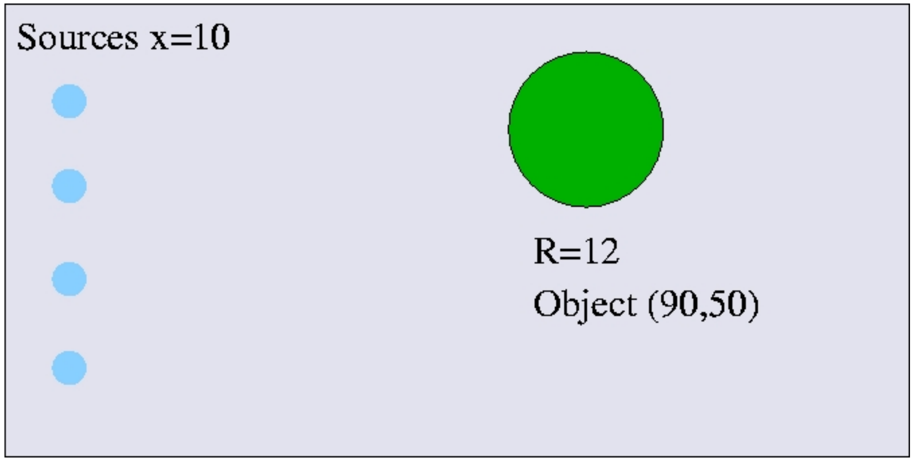

σ_{n}/a_0	error on R (%)	error on x_b	error on y_b
0.25%	12	9.0	3.5
0.5%	25	15	5.0
1%	33	30	10

Very accurate data are required to locate and estimate the inclusion.

TR in Changing media; forward stage

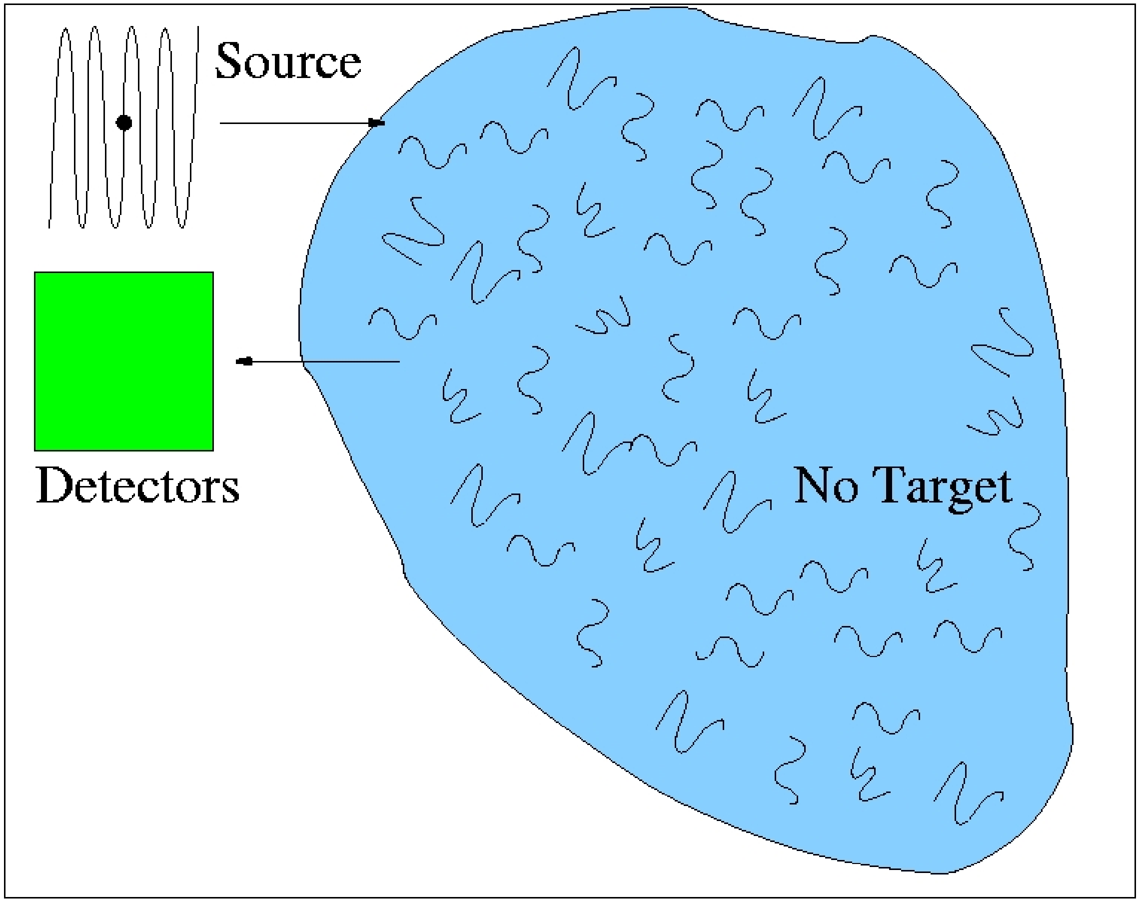

TR in changing media; backward stage

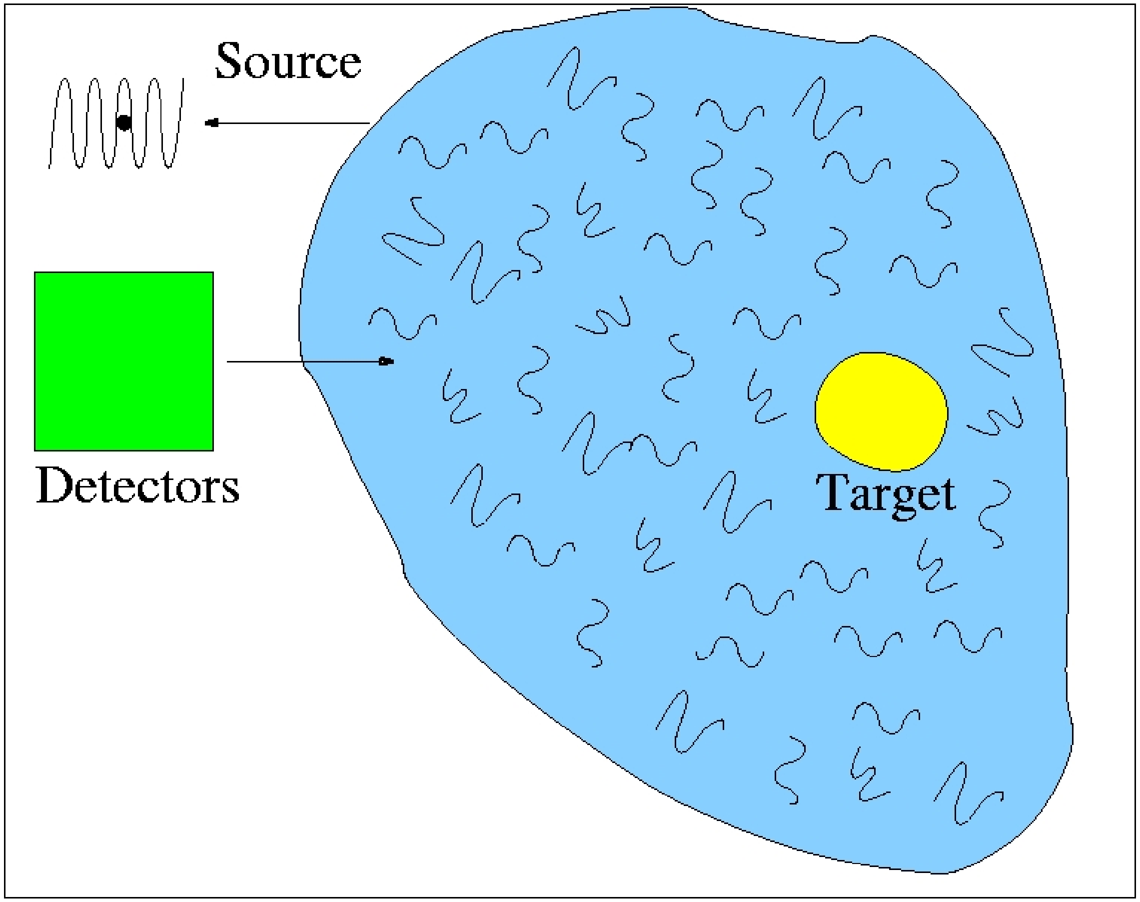

Imaging and changing media

In the diffusive regime, the perturbation caused by a void inclusion is given approximately by

$$\delta u^D(t,\mathbf{x}) = d\pi D_0 R^d \int_0^t \nabla_{\mathbf{x}} u_0(t-s,\mathbf{x}_b)\cdot\nabla_{\mathbf{x}_b} G(s,\mathbf{x},\mathbf{x}_b)ds.$$

Here d is dimension and $G(s,\mathbf{x},\mathbf{x}_b)$ the background Green's function. When we have access to the measured wave field **both** in the presence and in the absence of the inclusion, we can consider the correlation of the two fields. In the diffusive regime, the corresponding perturbation is given by

$$\delta u(t,\mathbf{x}) = -4\pi R \int_0^t u_0(t-s,\mathbf{x}_b) G(s,\mathbf{x},\mathbf{x}_b)ds + o(R), \qquad d=3$$

$$\delta u(t,\mathbf{x}) = \frac{2\pi}{\ln R} \int_0^t u_0(t-s,\mathbf{x}_b) G(s,\mathbf{x},\mathbf{x}_b)ds + o(\frac{1}{|\ln R|}), \qquad d=2.$$

Since $O(R) \gg O(R^3)$ in $d=3$ and $O(|\ln R|^{-1}) \gg O(R^2)$ in $d=2$, it is much easier to detect and image in the presence of differential information.

Can time-reversal experiments help?

Direct energy and time reversal measurements are hampered by two types of noise: background noise n_e and model noise n_m (characterizing the accuracy of the diffusive model). Let U be the direct measurement and F the TR filter measurement. Then we have that (after a few simplifications)

$$\begin{aligned} \delta\tilde{U} &= \delta U + n_m U_0 + n_d \\ \delta\tilde{F} &= \delta F + n_m F_0 + \varepsilon^{d/2} n_d; \quad (d \text{ is dimension}). \end{aligned}$$

Thus both types of measurements are equally affected by the model noise. However, because background noise does not refocus at the source location, it is strongly attenuated in the TR experiment.

In practice, direct measurements are very faint and thus even very small background noise renders the detection impossible. This is where time reversal helps (and may justify its equipment cost).

Conclusions

We have a theory to express the high frequency limit of the refocused signal in Time Reversal experiments using a Wigner transform. The filter can also be generalized to account for changing environments.

In certain cases, we can rigorously characterize the high frequency limit of the Wigner transform and obtain its statistical stability. This has been done for the parabolic approximation and the Itô Schrödinger approximation, and in the random Liouville regime.

Radiative transfer was shown to be quite accurate numerically to model wave propagation in (certain) random media.

Wave propagation is (often) sufficiently stable so that inverse problems based on transport equation can successfully be solved to detect and image buried inclusions. *Differential data* allow us to detect and image much *smaller* objects.

References

G.Bal and L.Ryzhik, *Time Reversal for Classical Waves in Random Media*, C. R. Acad. Sci. Paris, Série I, 333 (2001), 1041–1046

G.Bal and L.Ryzhik, *Time Reversal and Refocusing in Random Media*, SIAM J. Appl. Math. 63(5) (2003) 1475-1498

G.Bal and R.Verástegui, *Time Reversal in Changing Environment*, Multiscale Model. Simul., 2(4) (2004), 639-661

G.Bal and L.Ryzhik, *Stability of time reversed waves in changing media* Disc. Cont. Dyn. Syst. A 12(5) (2005), 793-815

G.Bal and O.Pinaud, *Time Reversal Based Detection in Random Media*, To appear in Inverse Problems

G.Bal and O.Pinaud, *Accuracy of transport models for acoustic waves in random media*, preprint